NeuroImage: Clinical 25 (2020) 102111

Contents lists available at ScienceDirect

NeuroImage: Clinical

journal homepage: www.elsevier.com/locate/ynicl

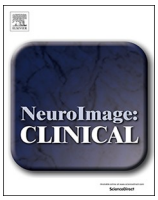

Predicting severity and prognosis in Parkinson's disease from brain microstructure and connectivity

Nooshin Abbasi[a,*], Seyed-Mohammad Fereshtehnejad[b,c,d], Yashar Zeighami[a], Kevin Michel-Herve Larcher[e], Ronald B. Postuma[b,f], Alain Dagher[a]

[a] McConnell Brain Imaging Centre, Montreal Neurological Institute, McGill University, 3801 University St., Montreal, Quebec H3A 2B4, Canada
[b] Department of Neurology and Neurosurgery, McGill University, Montreal, Quebec, Canada
[c] Division of Neurology, Department of Medicine, The Ottawa Hospital, University of Ottawa, Ottawa, Ontario, Canada
[d] Division of Clinical Geriatrics, Department of Neurobiology, Care Sciences and Society (NVS), Karolinska Institute, Stockholm, Sweden
[e] Biospective Inc., Montreal, Quebec, Canada
[f] Centre for Advanced Research in Sleep Medicine, Hôpital du Sacré-Coeur de Montréal, Montreal, Quebec, Canada

A B S T R A C T

Objectives: Investigating biomarkers to demonstrate progression of Parkinson's disease (PD) is of high priority. We investigated the association of brain structural properties with progression of clinical outcomes and their ability to differentiate clinical subtypes of PD.

Methods: A comprehensive set of clinical features was evaluated at baseline and 4.5-year follow-up for 144 *de-novo* PD patients from the Parkinson's Progression Markers Initiative. We created a global composite outcome (GCO) by combining z-scores of non-motor and motor symptoms, motor signs, overall activities of daily living and global cognition, as a single numeric indicator of prognosis. We classified patients into three subtypes based on multi-domain clinical criteria: 'mild motor-predominant', 'intermediate' and 'diffuse-malignant'. We analyzed diffusion-weighted scans at the early drug-naïve stage and extracted fractional anisotropy and mean diffusivity (MD) of basal ganglia and cortical sub-regions. Then, we employed graph theory to calculate network properties and used network-based statistic to investigate our primary hypothesis.

Results: Baseline MD of globus pallidus was associated with worsening of motor severity, cognition, and GCO after 4.5 years of follow-up. Connectivity disruption at baseline was correlated with decline in cognition, and increase in GCO. Baseline MD of nucleus accumbens, globus pallidus and basal-ganglia were linked to clinical subtypes at 4.5-year of follow-up. Disruption in sub-cortical networks associated with being subtyped as 'diffuse-malignant' versus 'mild motor-predominant' after 4.5 years.

Conclusions: Diffusion imaging analysis at the early *de-novo* stage of PD was able to differentiate clinical sub-types of PD after 4.5 years and was highly associated with future clinical outcomes of PD.

1. Introduction

Although Parkinson's disease is often conceived of as a homogenous disease, there are in fact radical differences in clinical manifestations and progression between patients (Simuni et al., 2018). With this in mind, there is a growing need for identifying biomarkers to predict the progression of PD.

Despite several investigations, discovery of an accurate biomarker for PD progression has been still elusive. Neuroimaging research advances over the past decades, however, have provided promising detailed knowledge of the brain pathology in several neurodegenerative disorders including PD (Pyatigorskaya et al., 2014, Lehéricy et al., 2004). In particular, Diffusion Tensor Imaging (DTI) has shown various structural abnormalities in PD patients compared to healthy controls. Microstructural damage of white matter integrity, in terms of decreased fractional anisotropy (FA) and increased mean diffusivity (MD) has been reported in several brain regions in PD (Cochrane and Ebmeier, 2013, Zhang et al., 2016). Combining DTI analysis with graph theory and further reconstruction of the brain networks has demonstrated disruption of the brain connectivity and widespread pattern of decreased efficiency in PD patients compared to healthy controls (Li et al., 2016, Li et al., 2017). Surprisingly, DTI-based imaging analysis has also succeeded in detecting early pathological brain changes of PD (Yoshikawa et al., 2004). Insufficiency of global neural connections has been recently reported in early stage de novo PD patients, by applying the graph theoretical analysis on DTI scans (Abbasi et al., 2018). Moreover, several DTI studies detected an abnormal pattern of PD subnetworks with reduced connectivity using the network-based statistic (NBS) (Zalesky et al., 2010), which primarily involved key components of the limbic system, basal ganglia and sensorimotor area

* Corresponding author.
E-mail address: Nooshin.abbasi@mcgill.ca (N. Abbasi).

https://doi.org/10.1016/j.nicl.2019.102111
Received 17 June 2019; Received in revised form 26 November 2019; Accepted 27 November 2019
Available online 28 November 2019

(Nigro et al., 2016).

In addition to baseline DTI findings, a 6-year longitudinal study demonstrated increased mean diffusivity in various brain regions and a positive correlation between increased diffusivity in the anterior putamen and PD motor progression (Chan et al., 2016).

Although few longitudinal investigations have been conducted, systematic longitudinal studies on comprehensive assessments of PD outcomes are still lacking. Considering the alterations of the diffusion properties and damage of white matter tracts, here we primarily aimed to explore whether DTI biomarkers and in particular, structural network properties at baseline, are associated with long-term motor and non-motor outcomes in patients with PD who were enrolled in the Parkinson's Progression Markers Initiative (PPMI) cohort (www.ppmi-info.org/data). In addition, we investigated if baseline DTI measures are able to distinct clinical subtypes of PD (Fereshtehnejad et al., 2017).

2. Methods

2.1. Participants

Participants of the current study were included from the PPMI cohort (Marek et al., 2011). The PPMI is an ongoing multicenter study consisting of clinical, genetic, biological and imaging measurements of more than 400 PD patients, designed with the goal of identifying disease biomarkers. Each participating PPMI site received approval from a local research ethics committee before study initiation and written informed consent forms were obtained from all subjects participating in the study. According to the inclusion criteria, de novo PD patients aged 30 years or older at the time of diagnosis with at least two of the following clinical features were eligible: resting tremor, bradykinesia, rigidity OR either asymmetric resting tremor or asymmetric bradykinesia. Additional inclusion criteria were a diagnosis of PD for 2 years or less at the time of screening; Hoehn and Yahr stage I or II at the baseline visit; confirmation of dopamine transporter deficit in neuroimaging assessments; and not expected to require PD medications within at least 6 months from the baseline visit. Patients with a history of PD medication use including levodopa, dopamine agonists, MAO-B inhibitors (e.g., selegiline, rasagiline), amantadine or other PD medications within 60 days of the baseline visit or having a clinical diagnosis of dementia -as determined by the investigator on the basis of the criteria developed by the Movement Disorders Society (MDS)- were excluded (Marek et al., 2011).

2.2. Clinical subtypes

We recently recommended guidelines for subtyping de novo PD subjects based on clinical features (Fereshtehnejad et al., 2017). Three distinct subtypes of PD were defined by hierarchical clustering based on a composite motor severity score and three main non-motor domains at baseline: REM sleep behavior disorder (RBD), dysautonomia, and cognitive impairment. The “mild motor-predominant” subtype consists of individuals with both composite motor and all non-motor symptom scores below the 75th percentile of severity (calculated from the same PPMI population). At the other end of the spectrum, two criteria categorized the “diffuse-malignant” subtype: individuals who scored > 75 th percentile in composite motor symptom score and at least one of the three non-motor domains or those who scored > 75th percentile in all three non-motor domains, regardless of the motor severity. The remaining cases were classified as the “intermediate” subtype. This classification was supported by differing rates of progression of clinical and structural imaging measures at 2.7 years. To investigate if baseline DTI analysis could predict shifting in clinical subtypes, we reclassified participants after 4.5 years of follow-up by using the updated reference percentile values derived from the score distribution of these motor and non-motor features.

Applying this comprehensive classification on PPMI participants, 422 PD subjects were subcategorized into one of three subtypes, mild-motor predominant, intermediate and diffuse-malignant. Among them, 152 patients had undergone DTI scan of the brain at the baseline visit. The scans underwent a basic quality control assessment by the Center for Imaging of Neurodegenerative Diseases (VA Medical Center, San Francisco, CA), and processed images were uploaded to the PPMI website. We also checked each scan visually for quality assessment. Thereafter, 8 participants that either had only one baseline DTI or failed the quality control were excluded from our study, so that 144 PD patients (82 mild-motor predominant, 48 intermediate and 14 diffuse-malignant on baseline classification) were included for the main analysis.

Table 1
Demographic and clinical characteristics of the study population (n = 144) at baseline and the end of follow-up (4.5 years).

Characteristic	Baseline	Follow-up
Demographics		
Age at onset (year)	60.6 (9.5)	–
Male sex (%)	90 (62.5%)	–
Education history (year)	15.3 (3.0)	–
Symptoms duration (month)	6.5 (6.8)	–
Positive family history (%)	24 (16.9%)	–
Clinical Motor Features		
UPDRS-Part II	5.5 (4.0)	10.2 (7.7)
UPDRS-Part III	20.6 (8.7)	27.9 (14.9)
Schwab & England score	94.6 (5.4)	86.2 (13.5)
PIGD score	0.22 (0.23)	0.51 (0.67)
Clinical Non-Motor Features		
UPDRS-Part I	5.2 (3.7)	7.6 (5.5)
Epworth sleepiness score	5.9 (3.3)	8.1 (5.1)
Geriatric depression scale (GDS)	2.4 (2.6)	3.3 (3.6)
State-trait anxiety inventory (STAI) score	66.6 (18.5)	67.8 (22.5)
Impulse control disorders (QUIP score)	0.28 (0.57)	0.33 (0.61)
REM sleep behavior disorder (RBD) score	3.3 (2.4)	4.8 (3.2)
SCOPA autonomic score	9.1 (6.0)	12.7 (6.7)
MOCA score	27.7 (2.1)	26.7 (4.1)

2.3. Clinical measures

A comprehensive set of demographic and clinical features were recorded at enrollment and at every follow-up visit for each participant. Table 1 summarizes the baseline and 4.5-year follow-up values for each clinical measure categorized into motor and non-motor manifestations.

For longitudinal assessments, we defined four major clinical outcomes consisting of:

- Motor severity: sum of the severity scores for motor symptoms and signs measured by the MDS-unified Parkinson's disease rating scale (MDS-UPDRS) (Goetz et al., 2008) parts II and III, respectively.
- Motor phenotype: postural instability gait difficulty (PIGD) score (Stebbins et al., 2013).
- Cognition: global cognitive status measured by the Montreal cognitive assessment (MoCA) score (Nasreddine et al., 2005).
- Global composite outcome (GCO): for analysis of overall disease progression, we used a previously-published global composite score as a single numeric indicator of prognosis (Fereshtehnejad et al., 2017, Fereshtehnejad et al., 2015). This was calculated by combining z-scores of: 1) non-motor symptoms (MDS-UPDRS-I), 2) motor symptoms (MDS-UPDRS-II), 3) motor signs (MDS-UPDRS-III), 4) overall activities of daily living (Schwab and England ADL) and 5) global cognition (MoCA score).

2.4. MRI acquisition

We used the initial visit whole-brain T1 structural and diffusion MRI scans of our participants which were performed at various sites on a

Siemens 3 Tesla TIM Trio system (Siemens AG, Munich, Germany) using a 12-channel Matrix head coil. According to the PPMI cohort imaging protocols a three-dimensional T1 image was acquired using a magnetization-prepared rapid acquisition gradient echo protocol with the following parameters: repetition time (TR) = 2300 ms; echo time (TE) = 2.98 ms; field of view (FOV) = 256 mm; flip angle = 9; and voxel size = 1 mm3. The whole-brain diffusion MRI acquisition sequence used the following parameters: diffusion gradient directions = 64; TR = 900 ms; TE = 88 ms; b-values = 0, 1000s/mm2; FOV = 230 × 230 mm; in-plane resolution = 2 mm isotropic; number of contiguous slices = 72; slice thickness = 2 mm; and acceleration factor = 2. Detailed acquisition parameters are available on the PPMI website (http://www.ppmi-info.org/study-design/research-documents-and-sops/).

2.5. DTI processing

Diffusion Weighted Imaging data were preprocessed and analyzed using the Oxford Center for Functional MRI of the Brain Diffusion Toolbox (v5.0) (http://www.fmrib.ox.ac.uk/fsl) (Smith et al., 2004). Visual quality assessment was performed after each processing step. Baseline diffusion-weighted scans were first corrected for head motion and eddy currents. Diffusion tensor models were then fitted independently for each voxel within the brain, and FA and MD maps were subsequently computed for each participant.

2.6. Fractional-anisotropy and mean-diffusivity maps

Using the previously extracted maps, we mainly focused on six regions of interest (ROI) in the basal ganglia including ventral caudate, dorsal caudate, globus pallidus, nucleus accumbens, ventromedial putamen and dorsolateral putamen and estimated the mean FA and MD in each hemisphere. FA and MD measures were then summed to obtain a whole basal ganglia measure for each hemisphere. Moreover, a previous structural study on the PPMI dataset revealed cortical thinning of various brain regions after 1 year of follow up in PD patients relative to healthy controls (Yau et al., 2018). Accordingly, we conducted an exploratory analysis on the seven affected cortical regions including bilateral medial and inferior frontal lobe, precentral and postcentral gyri, inferior and medial temporal lobe and left lateral occipital gyri. The results of the cortical analysis are presented in Supplementary material.

2.7. Brain parcellation

We used the Brainnetome atlas for brain parcellation (http://www.atlas.brainnetome.org) (Brainnetome , 2013). This atlas consists of 246 cortical and sub-cortical regions based on MRI-derived structural and functional connectivity patterns and cytoarchitecture. Brainnetome regions were non-linearly transformed into the DTI space of each participant using the FNIRT package of FSL. The affine transformation from a subject's native to the structural (T1 MRI) space followed by nonlinear warps/displacement of structural to standard (MNI152) space were calculated and inversely applied on the Brainnetome regions for each participant.

2.8. Network analysis

Interregional white matter tracts were analyzed using a multi-fiber diffusion probabilistic model which estimates probability distribution of one or more connections at each brain voxel using the probtrackx package of FSL (Behrens et al., 2007). Whole brain network construction was performed via tractography between each of the regional labels as a seed and the remaining labels as targets. Using the Brainnetome atlas parcellations, a 246 × 246 weighted interregional connectivity matrix was thus obtained for each participant. Each value within the connectivity matrices represents the number of probabilistic tracts or fiber pathways that connect the two regions. Since diagonal elements represent self-connections, we excluded them from further graph analyses. Thus, the nodes of the graph are the brain parcels and the edges the estimated number of white matter tracts between them.

2.9. Graph theoretical analysis

We used the Brain Connectivity Toolbox (http://www.braim-connectivity-toolbox.net/) (Rubinov and Sporns, 2010) to perform graph theoretical analysis on the individual brain graphs or connectomes. For each connectivity matrix we calculated the following global network measures: 1) global efficiency, the average of the inverse shortest path length; 2) mean clustering coefficient, the mean probability that two nodes connected to an index node are also connected with each other; 3) characteristic path length, the average shortest path length between any two nodes. We also examined the following local characteristics of the graph: 1) nodal degree, the number of connections of any node with the rest of the network; 2) nodal strength, the sum of weights of links connected to a node; 3) clustering coefficient, the fraction of a node's neighbors that are neighbors of each other; 4) local efficiency, the efficiency computed on node neighborhoods (Brainnetome , 2013). According to our primary hypothesis, assessments for the local metrics were performed on the 6 distinct basal ganglia sub-regions of each hemisphere based on the Brainnetome atlas parcellations.

2.10. Network-based statistic analysis

Given the fact that the mild motor-predominant and the diffuse-malignant subtypes represent the two extremes of PD clinical severity (Fereshtehnejad et al., 2017), we used the NBS analysis approach to further identify specific different interregional white matter subnetwork between the two subtypes, using clinical classification from the baseline and follow up visits (4.5 years). By evaluating the null hypothesis at the level of interconnected subnetworks rather than individual connections, we avoided multiple comparisons problems when mass univariate testing is performed at every connection in the graph. Zalesky et al. have provided a detailed description of the NBS methodology (Zalesky et al., 2010). Briefly, this method first identifies the supra-threshold connections by using a primary component-forming threshold. Then, the size of the remaining connected components in the network (i.e., number of edges) is determined. Using the null distribution of maximal connected component size obtained empirically by a non-parametric permutation approach, a corrected p-value is calculated. In addition, we re-did this analysis by weighting each connection by fractional anisotropy and mean diffusivity and re-calculated the connectivity matrices across PD subtypes. 5000 permutations were used for this analysis. These results are presented in Supplementary materials.

2.11. Statistical analysis

We used R v3.2.2 (RStudio Team 2015) and MATLAB v2108a to perform statistical analysis. We summed the left- and right- hemisphere values of FA and MD as a single aggregate measure. Global and local connectivity metrics were also calculated using the afore-mentioned graph analysis.

One-way ANOVA tests were used to compare differences in baseline DTI measures between various clinical subtypes of PD, defined at baseline and after 4.5 years of follow-up. A two-tailed FDR-corrected p-value < 0.05 was considered as the significance threshold for the comparative analyses.

Furthermore, we performed an exploratory Pearson correlation analysis to assess whether baseline DTI measures and network metrics associate with longitudinal change in the clinical outcomes of interest after follow-up. Afterwards, we regressed out the effect of age, as a

potential confounder, by adjusting all associations for age using partial correlations.

In order to investigate the primary drivers of the relationship between brain measures, demographic features and clinical outcomes in a single model, we performed a partial least square (PLS) analysis (Herve and Williams, 2010). PLS is a multivariate approach based on singular value decomposition (SVD) of the data matrices to investigate the linear relationship between two sets of variables. We used the PLS MATLAB toolbox (McIntosh and Lobaugh, 2004) (https://www.rotman-baycrest.on.ca/index.php?section=84). This approach was previously explained in detail elsewhere (Zeighami et al., 2017). Briefly, SVD was applied to the correlation matrix between two sets of measures (i.e. brain and clinical measures). The significance of the covariance explained for each latent variable was measured using permutation analysis ($N = 500$ repeats). The confidence interval for individual coefficients for each variable loaded in a given latent variable was calculated using bootstrapping (i.e. randomly sampled with replacement, $N = 500$). We ran the analysis with MD- and FA-only to ensure the stability of the results.

2.12. Data availability

All data used in this manuscript are part of publicly available and de-identified PPMI database (https://www.ppmi-info.org). Procedures for data request can be found at https://www.ppmi-info.org/access-data-specimens/download-data.

3. Results

The study population consisted of 90 (62.5%) males and 54 (37.5%) females with an average age of 60.6 (SD = 9.5) years and symptom duration of 6.5 (SD = 6.8) months at enrollment. Participants were all in the drug-naïve stage with an average MDS-UPDRS-part III score of 20.6 (SD = 8.7) and Hoehn and Yahr stage of 1–2 at baseline. Other demographic and clinical measures at baseline and after 4.5 years follow-up are listed in Table 1.

3.1. Clinical subtypes of PD

Using previously determined multi-domain criteria (Fereshtehnejad et al., 2017), 82 (56.9%) participants were categorized as 'mild motor-predominant', 48 (33.3%) as 'intermediate', and 14 (9.7%) as 'diffuse-malignant' at baseline. Whereas no single microstructural DTI measure in basal nuclei differentiated clinical subtypes at baseline (Fig. 1), network metrics significantly varied between the initial subtypes at enrollment (Fig. 2). Individuals with 'diffuse-malignant' PD at baseline had significantly lower global efficiency (FDR connected $p < 0.05$) and higher characteristic path length (FDR corrected $p < 0.05$, Fig. 2, Table 2a) compared to the other subtypes.

After 4.5 years of follow-up, 62% of patients remained in their subtype, and 38% of the study population switched clinical subtypes. At follow up, 83 (57.6%) were classified as 'mild motor-predominant', 45 (31.3%) as 'intermediate' and 16 (11.1%) as the 'diffuse-malignant' subtype. Differences between local metrics of basal ganglia across PD subtypes are presented in Table 2b. As illustrated in Fig. 1, mean diffusivity of nucleus accumbens (FDR corrected $p < 0.001$), globus pallidus (FDR corrected $p < 0.05$) and the entire basal ganglia (FDR corrected $p < 0.05$) at the baseline scan could significantly predict clinical subtypes at the 4.5 years of follow-up. Furthermore, participants who were categorized as 'diffuse-malignant' PD after 4.5 years, had significantly lower global efficiency (FDR corrected $p < 0.001$) and higher characteristic path length (FDR corrected $p < 0.001$) at baseline (Table 2a, Fig. 2)

We also compared nodal metrics of basal ganglia between PD subtypes (Supplementary Fig. e.1). Members of the 'diffuse-malignant' subtype, defined after 4.5 years follow-up, had significantly lower local efficiency of caudate, nucleus accumbens, and dorsolateral putamen at baseline (FDR corrected $p < 0.05$, Supplementary Fig. e.1). Individuals with 'diffuse-malignant' PD had significantly lower nodal strength in nucleus accumbens (FDR corrected $p < 0.05$).

Finally, for the cortical regions, at baseline only nodal strength of the pre-central ($P_{fdr} = 0.02$, mean sum of sub-regional z-scores: mild motor-predominant = 0.6871, intermediate = 0.8631, diffuse-malignant = −6.9840) and post-central ($P_{fdr} = 0.02$, mild motor-predominant = 0.9431, intermediate = −0.2281, diffuse-malignant = −4.9374) gyri were significantly lower in 'diffuse-malignant' subtype. Moreover, participants who were categorized as 'diffuse-malignant' PD after 4.5 years, had significantly higher mean diffusivity of inferior frontal ($P_{fdr} = 0.042$, mild motor-predominant = 0.0148, intermediate = 0.0149, diffuse-malignant = 0.0162) and medial ($P_{fdr} = 0.036$, mild motor-predominant = 0.0081, intermediate = 0.0081, diffuse-malignant = 0.0088) and inferior ($P_{fdr} = 0.018$, mild motor-predominant = 0.0127, intermediate = −0.0129, diffuse-malignant = 0.0136) temporal lobe and lower nodal strength in the seven cortical ROIs ($P_{fdr} < 0.05$).

3.2. Longitudinal progression in clinical outcomes

Table 3 and supplementary table e-1 summarize the results of the exploratory bivariate Pearson and age-adjusted partial correlations between DTI measures at baseline and longitudinal changes in the clinical outcomes of interest after follow-up focusing on the basal ganglia. Baseline mean diffusivity, in all regions, was associated with further increase in PIGD score (faster development of posture and gait problems); however, among basal ganglia nuclei, it remained statistically significant in globus pallidus after regressing out the effect of aging ($r = 0.25$, $p = 0.003$). Baseline mean diffusivity of globus pallidus was also significantly associated with the worsening of motor severity as measured by MDS-UPDRS-parts II-III ($r = 0.27$, $p = 0.001$), cognition as measured by MoCA ($r = -0.18$, $p = 0.040$), and global outcome as shown by the GCO z-score ($r = 0.30$, $p < 0.0001$) after 4.5 years of follow-up. As shown in Table 3, FA failed to demonstrate any significant association with disease progression.

After running the PLS analysis between MD/FA and the clinical measures, we found that the first latent variable significantly explained the covariance between the two sets of variables (Fig. 3). These results showed a relationship between generally higher mean diffusivity in basal ganglia and 1) older age, 2) male gender, 3) more rapid cognitive decline (further reduction in MOCA, 4) more rapid worsening of postural instability and gait (expressed in the PIGD score), and faster progression of global impairment (increased GCO score). The first latent variable accounted for 75% of the covariance. However, these results were mainly driven by the alterations in MD rather than FA, as shown on the previous analysis. In a post hoc analysis we ran PLS analysis separately, for MD and FA. The results were highly stable for MD-only, with a high degree of similarity to the original results, however the first latent variable for FA-only was not significant, indicating a higher contribution of MD to the original covariance explained. Finally, the relationship between MD and clinical measures was consistent and similar in different areas of basal ganglia in the PLS model. This suggests that the alteration in mean diffusivity could be present throughout the whole basal ganglia and not restricted to only one of its sub-components.

Investigating the brain network metrics, decreased global efficiency and increased characteristic path length at baseline significantly correlated with increase in GCO ($r = -0.19$ and $+0.18$ respectively, $p \leq 0.05$), increase in PIGD scores ($r = -0.30$ and $+0.32$ respectively, $p < 0.001$) and decline in MoCA ($r = +0.22$ and -0.22 respectively, $p < 0.05$) after follow-up. These associations remained statistically significant after regressing out the effect of aging (Table 3). In basal ganglia network, higher clustering coefficient and local efficiency at baseline correlated with less increase in PIGD score ($r = -0.19$ and

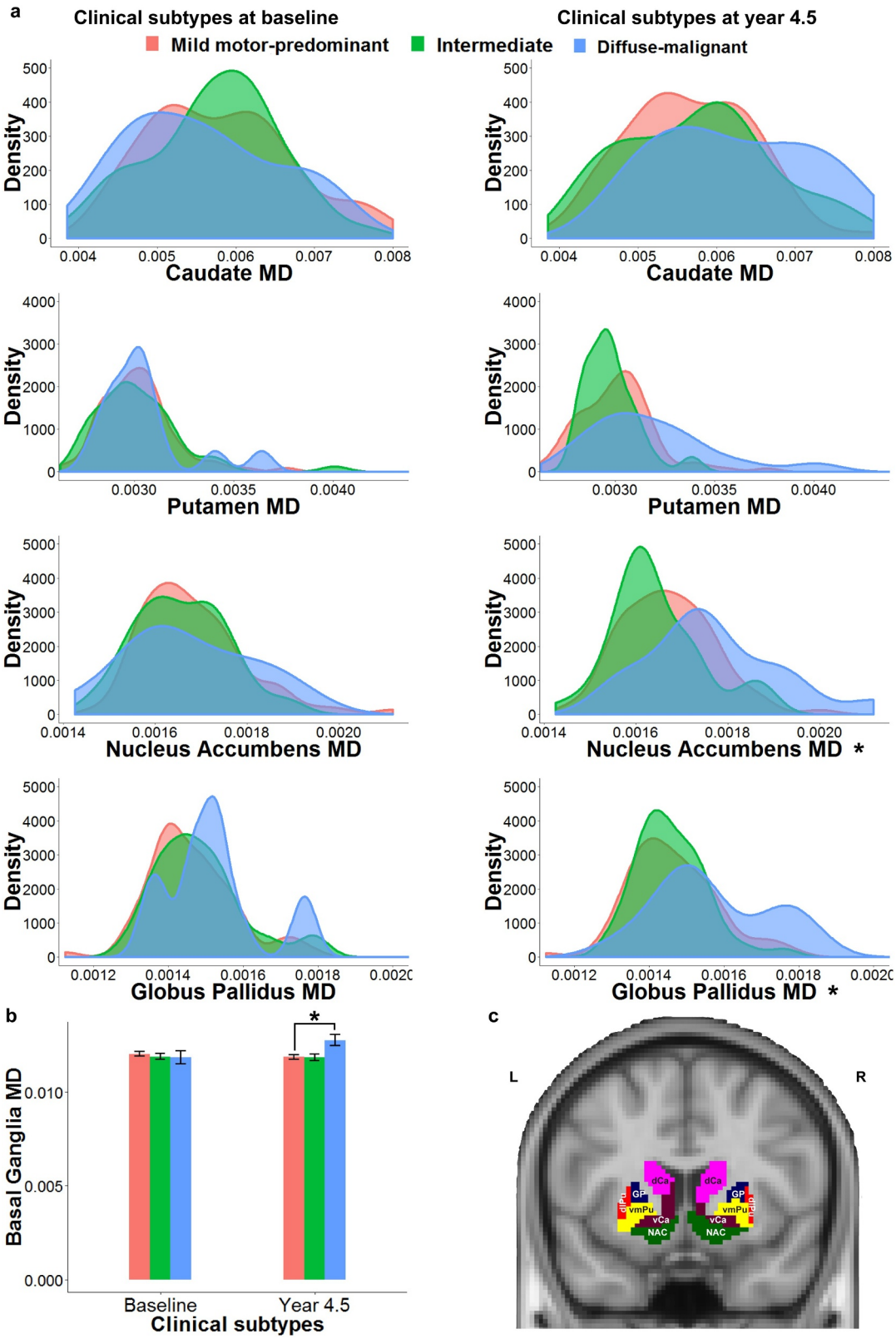

Fig. 1. Basal ganglia mean diffusivity in baseline and follow up subtypes of Parkinson's disease (PD)
(a) Mean diffusivity of basal ganglia sub-regions in baseline (left) and follow up (right) PD sub-types. Diffuse-malignant subtype, particularly after 4.5 years of follow up, showed higher mean diffusivity of nucleus accumbens and globus pallidus. (b) Mean diffusivity of basal ganglia in follow up diffuse-malignant subtype was significantly higher than the mild motor-predominant subtype, (c) Sub-regions of basal ganglia in Brainnetome atlas. MD = mean diffusivity, L = left, R = right, vCa = ventral caudate, GP = globus pallidus, NAC = nucleus accumbens, vmPu = ventromedial putamen, dCa = dorsal caudate, dlPu= dorsolateral putamen, * = p-value < 0.05.

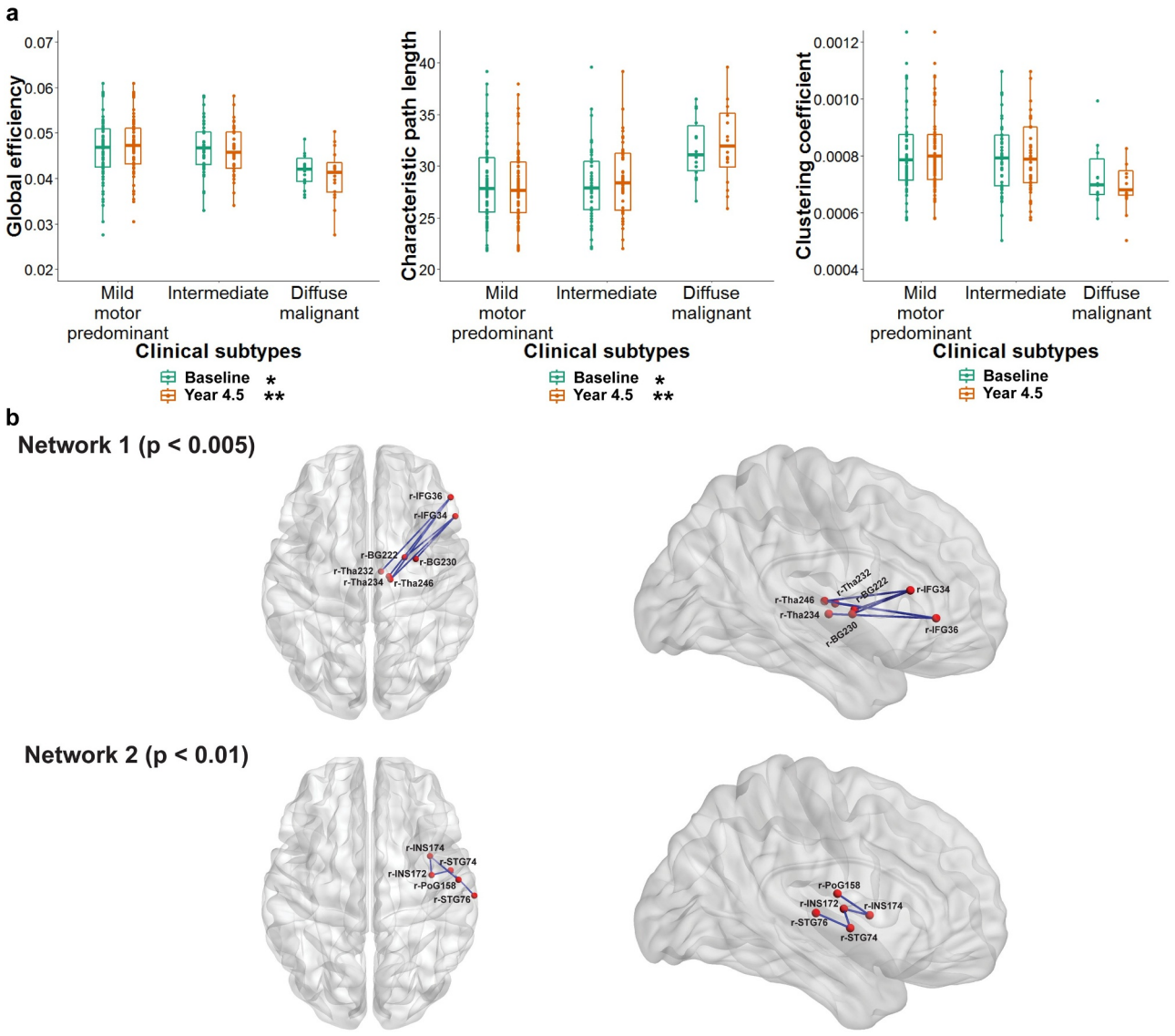

Fig. 2. Structural brain network and clinical subtypes of Parkinson's disease (PD)
(a) Global efficiency and characteristic path length showed more disruption in anatomical brain connectivity in diffuse-malignant subtype of PD. (b) Network based statistic identified two subnetworks with decreased efficiency in diffuse malignant compared to mild motor-predominant in the follow up clinical subtypes. The first subnetwork consisted of 6 edges, connecting 7 regions of the brain (corrected $p < 0.005$) which primarily involved key components of basal ganglia, thalamus and inferior frontal gyrus. The second subnetwork consisted of 5 brain sub-regions including insula and superior temporal gyrus which were connected through 4 edges (corrected $p < 0.01$). r = right hemisphere, IFG = inferior frontal gyrus, BG = basal ganglia, Tha = thalamus, INS = insula, STG = superior temporal gyrus, PoG = post-central gyrus.

-0.20, $p < 0.05$) and less decline in MoCA score ($r = 0.21$ and 0.21, $p < 0.05$) after 4.5 years. Participants with higher nodal strength of basal ganglia also experienced less cognitive decline after follow-up ($r = 0.25$, $p = 0.003$). The associations between baseline nodal metrics in basal ganglia and longitudinal change in MoCA and PIGD scores were independent of the effect of aging (Table 3).

Table 2a
Baseline global network measures between distinct clinical subtypes of Parkinson's disease, defined at baseline and after 4.5 years of follow-up ($n = 144$). (Values in each cell represent the average z-score of each measure in each subtype).

	Parkinson's disease clinical subtypes at baseline			
Global Network Metrics	**Mild Motor-predominant**	**Intermediate**	**Diffuse malignant**	**Corrected *p*-value $_{fdr}$**
Global efficiency	0.05527	0.12158	−0.7406	**0.033**
Characteristic path length	−0.0305	−0.1454	0.67711	**0.033**
Mean clustering coefficient	0.04291	0.01003	−0.2857	0.526
	Parkinson's Disease Clinical Subtypes at Follow-up			
Global Network Metrics	**Mild Motor-predominant**	**Intermediate**	**Diffuse malignant**	**Corrected *p*-value $_{fdr}$**
Global efficiency	0.17531	6.1E-06	−0.9094	< **0.001**
Characteristic path length	−0.1715	−0.0345	0.98657	< **0.001**
Mean clustering coefficient	0.05012	0.01606	−0.3052	0.428

Table 2b
Baseline local network measures of basal ganglia between distinct clinical subtypes of Parkinson's disease, defined at baseline and after 4.5 years of follow-up (n = 144).

(Values in each cell represent the average z-score of each measure in each subtype).

	Parkinson's Disease Clinical Subtypes at Baseline			
Basal Ganglia	**Mild Motor-predominant**	**Intermediate**	**Diffuse malignant**	**Corrected *p*-value $_{fdr}$**
Clustering Coefficient	0.07438	0.04798	−0.6	0.089
Nodal Degree	0.02361	0.05079	−0.3124	0.467
Nodal Strength	−0.0025	0.16234	−0.5419	0.089
Local Efficiency	0.07417	0.06427	−0.6548	0.089
	Parkinson's Disease Clinical Subtypes at Follow-up			
Basal Ganglia	**Mild Motor-predominant**	**Intermediate**	**Diffuse malignant**	**Corrected *p*-value $_{fdr}$**
Clustering Coefficient	0.14702	−0.0862	−0.5202	0.076
Nodal Degree	0.10286	−0.0636	−0.3548	0.216
Nodal Strength	0.10439	−0.0192	−0.4874	0.125
Local Efficiency	0.14992	−0.0807	−0.5508	0.076

We also explored how nodal metrics in each sub-region of the basal ganglia associated with the progression of clinical outcomes (Table e-1). Region-specific nodal metrics were mostly associated with the change in PIGD score and cognitive status. Among basal ganglia sub-regions, nodal metrics of dorsolateral putamen significantly correlated with worsening of all clinical measures, namely motor severity, gait and postural instability, cognitive status and the GCO. Nodal metrics of nucleus accumbens also significantly associated with longitudinal change in motor phenotype as measured by PIGD score and cognitive impairment after 4.5 years (Table e-1).

Studying the cortical ROIs, only mean diffusivity of inferior temporal lobe showed significant correlation with PIGD (P_{fdr} = 0.006, r = +0.302), MOCA (P_{fdr} = 0.01, r = −0.27) and GCO (P_{fdr} = 0.009, r = 0.323) scores. Network measurements revealed no correlation with clinical measures after correcting for multiple comparisons.

3.3. Whole brain mapping of PD subtypes

NBS detected two subnetworks of significantly reduced connectivity at the baseline connectomes, in patients who were later subtyped as 'diffuse-malignant' compared to the 'mild-motor predominant' patients by the 4.5 years follow up classification (p < 0.05, corrected for multiple comparisons; Fig. 2). The first subnetwork consisted of 6 edges, connecting 7 regions of the brain (corrected p < 0.005) which primarily involved key components of regions known to be involved in PD like basal ganglia, thalamus and inferior frontal gyrus sub-regions. The second significantly different subnetwork consisted of 5 brain regions including insula and superior temporal gyrus sub-regions of the

Table 3
Bivariate Pearson and age-adjusted partial correlations between microstructural/network metrics at baseline and longitudinal changes in the clinical outcomes of Parkinson's disease progression after 4.5 years of follow-up.

Imaging Measures	Motor severity **Δ UPDRS-II-III**	Motor phenotype **Δ PIGD Score**	Cognition **Δ MoCA Score**	GCO **Δ z-score**
Mean Diffusivity				
Caudate	NS	**+0.19 (0.022)**	NS	NS
	–	NS	–	–
Putamen	NS	**+0.18 (0.031)**	NS	**+0.19 (0.027)**
	–	NS	–	NS
Nucleus Accumbence	NS	**+0.21 (0.012)**	NS	NS
	–	NS	–	–
Globus Pallidus	**+0.27 (0.001)**	**+0.29 (0.001)**	**−0.18 (0.040)**	**+0.30 (< 0.001)**
	+0.24 (0.004)	**+0.25 (0.003)**	NS	**+0.26 (0.003)**
Basal Ganglia	NS	**+0.25 (0.002)**	NS	**+0.21 (0.012)**
	–	**+0.19 (0.026)**	–	NS
Fractional Anisotropy				
Caudate	NS	NS	NS	NS
	–	–	–	–
Putamen	NS	NS	NS	NS
	–	–	–	–
Nucleus Accumbence	NS	NS	NS	NS
	–	–	–	–
Globus Pallidus	NS	NS	NS	NS
	–	–	–	–
Basal Ganglia	NS	NS	NS	NS
	–	–	–	–
Network Metrics				
Global Efficiency	NS	**−0.30 (< 0.001)**	**+0.22 (0.008)**	**−0.19 (0.026)**
	–	**−0.28 (0.001)**	**+0.21 (0.015)**	**−0.17 (0.052)**
Characteristic Path Length	NS	**+0.318 (< 0.001)**	**−0.22 (0.009)**	**+0.18 (0.031)**
	–	**+0.30 (< 0.001)**	**−0.20 (0.015)**	NS
Average of Clustering Coefficient	NS	NS	NS	NS
Nodal Metrics-Basal Ganglia				
Clustering Coefficient	NS	**−0.19 (0.022)**	**+0.21 (0.011)**	NS
	–	**−0.20 (0.016)**	**+0.23 (0.006)**	–
Nodal Degree	NS	NS	NS	NS
	–	**−0.21 (0.015)**	–	–
Nodal Strength	NS	NS	**+0.22 (0.004)**	NS
	–	–	**+0.28 (0.001)**	–
Local Efficiency	NS	**−0.20 (0.014)**	**+0.21 (0.011)**	NS
	–	**−0.22 (0.011)**	**+0.23 (0.006)**	**−0.17 (0.045)**

In each cell, data are presented as correlation coefficient (p-value) followed by age-adjusted values in the second row. Data on fractional anisotropy and mean diffusivity sections are incorporated as sum of the left- and right-side values. Correlations that remained statistically significant are bolded. GCO = Global Composite Outcome, UPDRS = Unified Parkinson's disease Rating Scale, MoCA = Montreal Cognitive Assessment, **Δ** = change in the clinical outcome, NS = not significant.

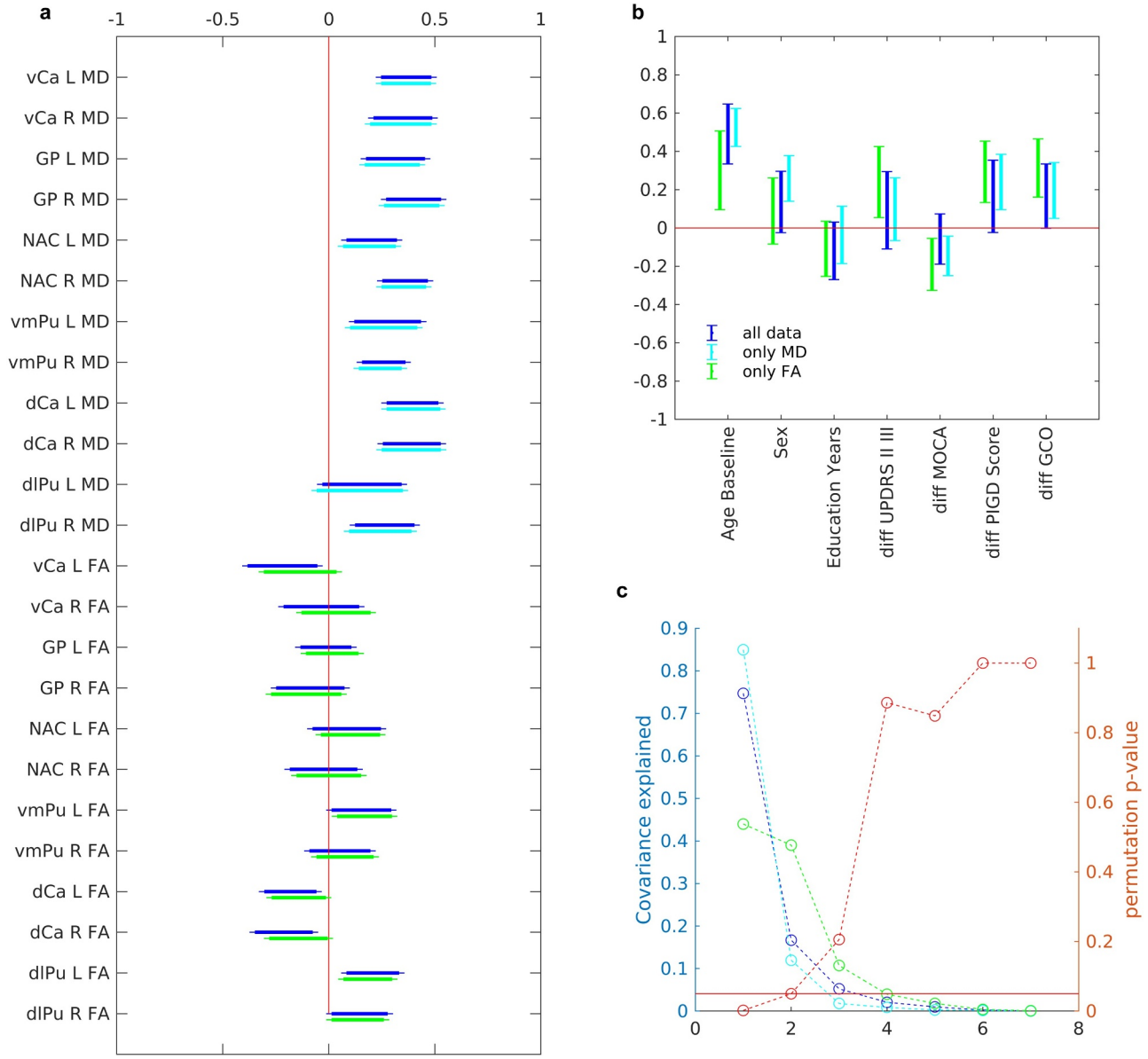

Fig. 3. Relationship between microstructural properties of brain and clinical measures (a) Regional microstructural properties contributing to the first latent variable using partial least square analysis. The confidence intervals calculated using bootstrapping (N = 500). (b) Clinical measures contributing microstructural properties to the first latent variable. (c) P-value based on the permutation analysis (N = 500), as well as covariance explained for each latent variable. In all plot blue is the main analysis using both mean diffusivity and fractional anisotropy, cyan is for using only mean diffusivity, and green is using only fractional anisotropy (The only mean diffusivity and only fractional anisotropy are only intended as post-hoc analysis for stability of results). L = left, R = right, vCa = ventral caudate, GP = globus pallidus, NAC = nucleus accumbens, vmPu = ventromedial putamen, dCa = dorsal caudate, dlPu = dorsolateral putamen.

Table 4
Networks identified to be significantly different between the “diffuse-malignant” and “mild-motor predominant” subtypes of Parkinson's disease, based on the 4.5-years follow up classification by using the Network-Based Statistical analysis.

Networks and connections	*t* value
Network 1 (7 nodes, 6 edges, p = 0.003)	
Right inferior frontal gyrus, caudal area 45 and Right globus pallidus	t = 3.03
Right Inferior frontal gyrus, caudal area 45 and Right dorsolateral putamen	t = 2.94
Right Inferior frontal gyrus, rostral area 45 and Right medial pre-frontal thalamus	t = 2.97
Right Inferior frontal gyrus, rostral area 45 and Right pre-motor thalamus	t = 3.23
Right Inferior frontal gyrus, caudal area 45 and Right lateral pre-frontal thalamus	t = 3.01
Right Inferior frontal gyrus, rostral area 45 and Right lateral pre-frontal thalamus	t = 2.90
Network 2 (5 nodes, 4 edges, p = 0.009)	
Right superior temporal gyrus TE1.0-TE1.2 and Right superior temporal gyrus, caudal area 22	t = 3.72
Right superior temporal gyrus TE1.0-TE1.2 and Right dorsal granular insula	t = 3.46
Right post-central gyrus and Right dorsal dys-granular insula	t = 3.13
Right dorsal granular insula and Right dorsal dys-granular insula	t = 3.61

barainnetome parcellation which were connected through 4 edges (Table 4). On the other hand, the FA-weighted connectivity matrices revealed no difference across a wide range of thresholds between the diffuse-malignant and mild motor-predominant subtypes of PD, defined at baseline and after 4.5 years. However, the MD-weighted connectome demonstrated three sub-networks with higher mean diffusivity in diffuse-malignant subtype of PD defined after 4.5 years of follow up compared to mild motor-predominant subtype. Similarly, basal ganglia, insula, cingulate and pre and post-central gyri were notably involved in different sub-networks of the MD-weighted matrices (Supplementary material).

4. Discussion

Having explored a large DTI set of early-phase, drug-naïve PD patients, our study provided new evidence that these measures of structural neural disruption can predict clinical motor and non-motor outcomes of PD. In this longitudinal cohort, we analyzed microstructural damage of regional integrity (reflected by increased diffusivity) and disruption of the brain's connectivity pattern predicted progression of motor and non-motor symptoms over time. The fact that baseline DTI properties could identify clinically distinct sub-types of PD patients after 4.5 years of follow up, highlights a key role for DTI biomarkers in classifying and predicting PD prognosis over time.

4.1. Microstructural abnormalities and PD progression

Disruption in coherence of the underlying brain tissue is mainly reflected by a decrease in FA or an increase in MD. Although for most of the brain regions decreased FA and increased MD occur together in a similar pattern, in some regions one measure dominates, as FA is more sensitive to tissue directionality, while MD mainly represents tissue density and extracellular fluid accumulation (Wiltshire et al., 2010). Disruption of the white matter integrity occurs in PD across several regions of the cerebral white matter and is particularly notable in subcortical areas (Pyatigorskaya et al., 2014, Cochrane and Ebmeier, 2013, Atkinson-Clement et al., 2017, Deng et al., 2018). Focusing on the basal ganglia and in line with pathologic pattern of PD development, we found significant associations between increased mean diffusivity of the basal ganglia sub-regions (particularly globus pallidus) at the very early de novo stage, and progression of global composite outcome after 4.5 years of follow up. The baseline MD value of globus pallidus also positively correlated with motor and cognitive progression and faster development of gait problems as measured by PIGD scoring. We did not find the same association for FA, a finding that was largely replicated by the PLS analysis. Several studies reported positive correlation between DTI measures of nigrostriatal projection loss and motor severity in PD (Yoshikawa et al., 2004, Zhang et al., 2015, Zhan et al., 2012); however, other studies did not replicate the association (Vaillancourt et al., 2009, Du et al., 2011). Zhang et al. reported higher rates of FA reduction and radial and axial diffusivity increases predominately in substantia nigra, midbrain and thalamus of PD patients in the same cohort (PPMI), after one year of follow up, compared to normal aging. They also observed that a steep increase in diffusivity of thalamus correlated with fast cognitive decline measured by MoCA; however, they found no significant correlation between microstructural DTI changes and UPDRS score after one year (Zhang et al., 2016). Previous studies on PD showed that cognitive impairment in executive and visuospatial domains associated with increases in diffusivity of thalamic (Chen et al., 2017), prefrontal (Auning et al., 2014) and frontal (Koshimori et al., 2015) regions. Zheng et al. reported that MD of various subcortical regions associated more strongly with performance in distinct cognitive domains than FA (Zheng et al., 2014). In addition, MD in putamen was positively correlated with MDS-UPDRS motor score (Wang et al., 2015) as well as MDS-UPDRS motor progression over 6 years (Chan et al., 2016). PD patients with freezing of gait showed higher MD values in subcortical structures such as basal ganglia compared to patients without gait freezing (Youn et al., 2015). It is interesting to note that the highest correlation of DTI changes with PD progression over 4.5-years of follow up was found for globus pallidus, which has a primary action in movement regulation and is used as a target for deep brain stimulation in PD (Dostrovsky et al., 2002). This is in line with previous results which showed a significant increase in diffusivity of the globus pallidus in PD patients compared to healthy controls (Atkinson-Clement et al., 2017, Menke et al., 2013) and its correlation with motor severity in the PIGD subtype of PD (Nagae et al., 2016).

In general, disruption of motor and cognitive function in PD may be related to more severe loss of brain tissue as reflected by diffusivity, than by disruption in tissue coherence (Zheng et al., 2014, Wang et al., 2015). Taken together, our results may suggest that baseline microstructural alterations of the brain regions, measured by increased diffusivity are not only correlated with major symptoms of PD (Hall et al., 2016) but also predict long term motor and non-motor outcomes of PD.

4.2. Structural network properties and PD progression

Implementing graph theoretical analysis, our results revealed significant correlations between baseline structural brain networks and future clinical outcomes of PD. Several studies have previously noted disruption of anatomical brain networks in PD patients compared to healthy controls (Nigro et al., 2016, Kamagata et al., 2018). More specifically, PD patients have demonstrated decreased efficiency of various global and local metrics of structural connections. In PPMI, PD patients have been shown to have disrupted structural connectivity at the global level compared to healthy controls (Abbasi et al., 2018). Few connectomic analyses have also investigated the correlation between altered brain networks and clinical manifestations in PD and reported that impaired cognition is associated with disruption of functional and structural brain networks (Christopher and Strafella, 2013, Beyer et al., 2013). Similar studies could not replicate such associations for severity of motor symptoms (Nigro et al., 2016, Fang et al., 2017, Campbell et al., 2015), resulting in general lack of consensus on the association of brain networks and clinical manifestations in PD. In the current longitudinal study, however, we observed remarkable links between baseline structural network metrics and clinical features of PD, both at the early drug-naïve stage and after 4.5 years of follow-up. Decreased global efficiency and increased characteristic path length which reflect disruption in the integration of brain connections were correlated with worsening of PIGD, MoCA and GCO scores after 4.5 years of follow up. Considering the key role of basal ganglia in PD, we observed that disruption of the local network metrics including clustering coefficient, local efficiency, nodal strength and degree in basal ganglia components, substantially correlated with progression of various motor and non-motor symptoms. These findings suggest that damages of structural connectivity pattern, either globally or locally in basal ganglia sub-regions, contribute to various clinical manifestations of PD. In other words, we found that similar to other neurodegenerative disorders (Tucholka et al., 2018, Daianu et al., 2013), structural connectivity pattern of the brain alters in early stages of PD and is correlated with clinical progression of the disease over time, as reflected in our graph theoretical analyses.

4.3. DTI and clinical subtypes of PD

Our results showed that DTI properties could significantly discriminate PD patients with different clinical subtypes after 4.5 years of follow up. Patients in the ‘diffuse-malignant’ subtype at baseline had increased diffusivity of basal ganglia and more disruption in global and local connectivity patterns, relative to the other subtypes. Indeed, clinical manifestations of PD directly associated with a distinct pattern of DTI properties. In general, microstructural and connectomic analyses

followed a disruptive trend as clinical symptoms were more severe from 'mild-motor predominant' to 'diffuse-malignant' subtype (Supplementary Fig. e.1).

In addition, our NBS analyses demonstrated a distinct brain network characterizing the structural connectivity abnormalities in the 'diffuse-malignant' subtype compared to 'mild motor-predominant' PD. The involved anatomical regions were predominantly pathways related to basal ganglia, thalamus and insula which is relatively consistent with spread of PD neurodegeneration.

The challenge of great heterogeneity in clinical manifestations of PD is largely illuminated by demonstrating differences in microstructural, graph theoretical and NBS analyses of DTI measures between distinct PD subtypes. These findings also provide additional validity for multi-domain classification of PD. Nevertheless, the fact that baseline DTI measures and network metrics were more prominently different between subtypes that were defined after 4.5 years follow-up clinical evaluations than those defined at baseline, highlights the potential of imaging biomarkers data to further optimize subtyping in PD.

4.4. Limitations and strengths

This study has several limitations. Our study was restricted to PPMI subjects and 3T imaging, so DTI studies with different protocols or imaging acquisition of higher fields may reveal additional details. Some technical limitations are inherent in multi-center studies, which PPMI has minimized by setting guidelines for data gathering. Another potential limitation is the choice of region of interest; additional group differences may be observable with analysis of other brain regions.

On the other hand, the current study has several strengths. We were able to study a large sample size of de novo PD patients enrolled at PPMI centers across the world which enhances generalizability of our findings. Also, here we have investigated basal ganglia sub-regions in detail by employing the Brainnetome atlas, which allowed us to clarify the contributions of particular sub-regions in pathophysiology of PD manifestations. Furthermore, we applied PLS as an innovative approach and the findings were consistent with our primary analyses, demonstrating a low possibility for multiple comparison bias. Finally, to the best of our knowledge, this is the first study that investigated the relationship between comprehensively-defined PD outcomes and different PD phenotypes to DTI MRI properties, on a large sample of PD patients over time.

Disclosure

None

Declaration of Competing Interest

None.

Acknowledgments

AD received funding from the Canadian Institutes for Health Research (grant number FDN-143242), Natural Sciences and Engineering Research Council of Canada, Michael J. Fox Foundation, Weston Brain Institute, and the Alzheimer Association. NA received funding from Preston Robb Fellowship from Montreal Neurological Institute. PPMI—a public-private partnership—is funded by the Michael J. Fox Foundation for Parkinson's Research and funding partners, including AbbVie, Avid, Biogen, Bristol-Myers Squibb, Covance, GE Healthcare, Genentech, GlaxoSmithKline, Lilly, Lundbeck, Merck, Meso Scale Discovery, Pfizer, Piramal, Roche, Sanofi Genzyme, Servier, Teva, and UCB. The funders had no role in study design, data collection and analysis, decision to publish, or preparation of the manuscript.

Supplementary materials

Supplementary material associated with this article can be found, in the online version, at doi:10.1016/j.nicl.2019.102111.

References

Simuni, T., Siderowf, A., Lasch, S., et al., 2018. Longitudinal change of clinical and biological measures in early Parkinson's disease: parkinson's progression markers initiative cohort. Mov. Disord. 33, 771–782.
Pyatigorskaya, N., Gallea, C., Garcia-lorenzo, D., Vidailhet, M, 2014. A review of the use of magnetic resonance imaging in Parkinson's disease. Ther. Adv. Neurol. Disord. 7 (4), 206–220.
Lehéricy, S., Ducros, M., De, Moortele PF Van, et al., 2004. Diffusion tensor fiber tracking shows distinct corticostriatal circuits in humans. Ann. Neurol. 55 (4), 522–529.
Cochrane, C.J., Ebmeier, K.P., 2013. systematic review and meta-analysis diffusion tensor imaging in Parkinsonian syndromes a systematic review and meta-analysis. Neurology 80 (9), 857–864.
Zhang, Y., Wu, I., Tosun, D., Foster, E., Schuff, N., 2016. Progression of regional microstructural degeneration in Parkinson's disease : a multicenter diffusion tensor imaging study. PLoS ONE 11 (10), e0165540.
Li, C., Huang, B., Zhang, R., Ma, Q., Yang, W, 2016. Impaired topological architecture of brain structural networks in idiopathic Parkinson's disease : a DTI study. Brain Imaging Behav. 11 (1), 113–128.
Li, X., Ren, Y., Cao, B., Huang, X, 2017. Analysis of white matter characteristics with tract-based spatial statistics according to diffusion tensor imaging in early Parkinson's disease. Neurosci. Lett. 675, 127–132.
Yoshikawa, K., Nakata, Y., Yamada, K., Nakagawa, M, 2004. Early pathological changes in the Parkinsonian brain demonstrated by diffusion tensor MRI. J. Neurol. Neurosurg. Psychiatry 75, 481–484.
Abbasi, N., Mohajer, B., Abbasi, S., Hasanabadi, P, 2018. Relationship between cerebrospinal fluid biomarkers and structural brain network properties in Parkinson's disease. Mov. Disord. 33 (3), 431–439.
Zalesky, A., Fornito, A., Bullmore, E.T., 2010. Network-based statistic: identifying differences in brain networks. Neuroimage 53, 1197–1207.
Nigro, S., Riccelli, R., Passamonti, L., et al., 2016. Characterizing structural neural networks in de novo Parkinson disease patients using diffusion tensor imaging. Hum. Brain Mapp. 37, 4500–4510.
Fereshtehnejad, S.M., Zeighami, Y., Dagher, A., Postuma, R.B, 2017. Clinical criteria for subtyping Parkinson's disease: biomarkers and longitudinal progression. Brain 140 (7), 1959–1976.
Marek, K., Jennings, D., Lasch, S., et al., 2011. The Parkinson Progression Marker Initiative (PPMI). Prog. Neurobiol. 95, 629–635.
Goetz, C.G., Tilley, B.C., Shaftman, S.R., et al., 2008. Movement disorder society-sponsored revision of the unified Parkinson's disease rating scale (MDS-UPDRS): scale presentation and clinimetric testing results. Mov. Disord. 23, 2129–2170.
Stebbins, G.T., Goetz, C.G., Burn, D.J., Jankovic, J., Khoo, T.K., Tilley, B.C, 2013. How to identify tremor dominant and postural instability/gait difficulty groups with the movement disorder society unified Parkinson's disease rating scale: comparison with the unified Parkinson's disease rating scale. Mov. Disord. 28, 668–670.
Nasreddine, Z.S., Phillips, N.A., Bedirian, V., et al., 2005. The Montreal Cognitive Assessment, MoCA: a brief screening tool for mild cognitive impairment. J. Am. Geriatr. Soc. 53, 695–699.
Fereshtehnejad, S.-M., Romenets, S.R., Anang, J.B.M., Latreille, V., Gagnon, J.-F., Postuma, R.B, 2015. New clinical subtypes of Parkinson disease and their longitudinal progression. JAMA Neurol. 72, 863.
Smith, S.M., Jenkinson, M., Woolrich, M.W., et al., 2004. Advances in functional and structural MR image analysis and implementation as FSL. Nueroimage 23 Suppl (1), S208–S219.
Yau, Y., Zeighami, Y., Baker, T.E., et al., 2018. Network connectivity determines cortical thinning in early Parkinson's disease progression. Nat. Commun. 9 (1), 12.
Brainnetome, J.T.N., 2013. A new -ome to understand the brain and its disorders. Neuroimage 80, 263–272.
Behrens, T.E.J., Berg, H.J., Jbabdi, S., Rushworth, M.F.S., Woolrich, M.W., 2007. Probabilistic diffusion tractography with multiple fibre orientations: what can we gain? Neuroimage 34, 144–155.
Rubinov, M., Sporns, O., 2010. Complex network measures of brain connectivity: uses and interpretations. Neuroimage 52, 1059–1069.
RStudio Team, 2015. RStudio. Integrated Development for R. RStudio, Inc., Boston, MA URL. http://www.rstudio.com/.
Herve, A., Williams, L.J., 2010. Principal component analysis. Comput. Stat. 2, 433–459.
McIntosh, A.R., Lobaugh, N.J., 2004. Partial least squares analysis of neuroimaging data: applications and advances. Neuroimage 23 Suppl (1), S250–S263.
Zeighami, Y., Fereshtehnejad, S.-M., Dadar, M., et al., 2017. A clinical-anatomical signature of Parkinson's disease identified with partial least squares and magnetic resonance imaging. Neuroimage 190, 69–78 S1053-8119(17)31074-1.
Wiltshire, K., Concha, L., Gee, M., Bouchard, T., Beaulieu, C., Camicioli, R, 2010. Corpus callosum and cingulum tractography in Parkinson's disease. Can. J. Neurol. Sci. 37, 595–600.
Atkinson-Clement, C., Pinto, S., Eusebio, A., Coulon, O., 2017. Diffusion tensor imaging in Parkinson's disease: review and meta-analysis. NeuroImage Clin. 16, 98–110.
Deng, X.-Y., Wang, L., Yang, T.-T., Li, R., Yu, G, 2018. A meta-analysis of diffusion tensor imaging of substantia nigra in patients with Parkinson's disease. Sci. Rep. 8, 2941.
Zhang, Y., Wu, I., Buckley, S., et al., 2015. Diffusion tensor imaging of the nigrostriatal

fibers in Parkinson's disease. Mov. Disord. 30, 1229–1236.
Zhan, W., Kang, G.A., Glass, G.A., et al., 2012. Regional alterations of brain microstructure in Parkinson's disease using diffusion tensor imaging. Mov. Disord. 27 (1), 90–97.
Vaillancourt, D.E., Spraker, M.B., Prodoehl, J., et al., 2009. High-resolution diffusion tensor imaging in the substantia nigra of de novo Parkinson disease. Neurology 72, 1378.
Du, G., Lewis, M.M., Styner, M., et al., 2011. Combined R2* and diffusion tenser imaging changes in the substantia nigra in Parkinson disease. Mov. Disord. 26, 1627–1632.
Chan, L., Ng, K., Yeoh, C., Rumpel, H., Li, H., Tan, E., 2016. Putaminal Diffusivity Correlates With Disease Progression in Parkinson's Disease. Medicine (Baltimore) 95 (6), e2594.
Chen, Y., Chen, M., Lu, C., et al., 2017. Associations among cognitive functions, plasma DNA, and white matter integrity in patients with early-onset Parkinson's disease. Front. Neurosci. 11, 9.
Auning, E., Kjærvik, V.K., Selnes, P., et al., 2014. White matter integrity and cognition in Parkinson's disease : a cross-sectional study. BMJ Open 4, e003976.
Koshimori, Y., Segura, B., Christopher, L., Lobaugh, N, 2015. Imaging changes associated with cognitive abnormalities in Parkinson's disease. Brain Struct. Funct. 220 (4), 2249–2261.
Zheng, Z., Shemmassian, S., Wijekoon, C., Kim, W., Bookheimer NP, S., 2014. DTI correlates of distinct cognitive impairments in Parkinson's disease. Hum. Brain Mapp. 35 (4), 1325–1333.
Wang, J., Yang, Q.X., Sun, X., et al., 2015. Parkinsonism and related disorders mri evaluation of asymmetry of nigrostriatal damage in the early stage of early-onset Parkinson's disease. Parkinsonism Relat. Disord. 21 (6), 590–596.
Youn, J., Lee, J.M., Kwon, H., Sun, J., Ok, T., Whan, J, 2015. Parkinsonism and related disorders alterations of mean diffusivity of pedunculopontine nucleus pathway in Parkinson's disease patients with freezing of gait. Parkinsonism Relat. Disord. 21 (1), 12–17.
Dostrovsky, J.O., Hutchison, W.D., Lozano, A.M, 2002. The globus pallidus, deep brain stimulation, and Parkinson's disease. Neuroscientist 8 (3), 284–290.
Menke, R.A.L., Szewczyk-krolikowski, K., Jbabdi, S., et al., 2013. Comprehensive morphometry of subcortical grey matter structures in early-stage Parkinson's disease. Hum. Brain Mapp. 35 (4), 1681–1690.
Nagae, L.M., Honce, J.M., Tanabe, J., Shelton, E., Sillau, S.H., Berman, B.D, 2016. Microstructural changes within the basal ganglia differ between Parkinson disease subtypes. Front. Neuroanat. 10, 17.
Hall, J.M., Ehgoetz, K.A., Walton, C.C., et al., 2016. Parkinsonism and related disorders diffusion alterations associated with Parkinson's disease symptomatology : a review of the literature. Parkinsonism Relat. Disord. 33, 12–26.
Kamagata, K., Zalesky, A., Hatano, T., et al., 2018. Connectome analysis with di ff usion MRI in idiopathic Parkinson's disease: evaluation using multi-shell, multi-tissue, constrained spherical deconvolution. NeuroImage Clin. 17, 518–529.
Christopher, L., Strafella, A.P., 2013. Neuroimaging of brain changes associated with cognitive impairment in Parkinson's disease. J. Neuropsychol. 7, 225–240.
Beyer, M.K., Bronnick, K.S., Hwang, K.S., et al., 2013. Verbal memory is associated with structural hippocampal changes in newly diagnosed Parkinson's disease. J. Neurol. Neurosurg. Psychiatry 84, 23–28.
Fang, J., Chen, H., Cao, Z., et al., 2017. Impaired brain network architecture in newly diagnosed Parkinson's disease based on graph theoretical analysis. Neurosci. Lett. 14 (657), 151–158.
Campbell, M.C., Koller, J.M., Snyder, A.Z., Kotzbauer, P.T., 2015. CSF proteins and resting-state functional connectivity in Parkinson disease. Neurology 84, 2413–2422.
Tucholka, A., Grau-Rivera, O., Falcon, C., et al., 2018. Structural connectivity alterations along the Alzheimer's disease continuum: reproducibility across two independent samples and correlation with cerebrospinal fluid amyloid-β and tau. J. Alzheimers Dis. 61 (4), 1575–1587.
Daianu, M., Jahanshad, N., Nir, T.M., et al., 2013. Breakdown of brain connectivity between normal aging and Alzheimer's disease: a structural *k* -Core network analysis. Brain Connect. 3, 407–422.